2009

High-Resolution, Long-Term Characterization of Bacterial Motility Using Optical Tweezers

Lon Chubiz, *University of Missouri-St. Louis*
Taejin L. Min, *University of Illinois at Urbana–Champaign*
Patrick J. Mears, *University of Illinois at Urbana–Champaign*
Christopher V. Rao, *University of Illinois at Urbana–Champaign*
Ido Golding, *University of Illinois at Urbana–Champaign*, et al.

High-resolution, long-term characterization of bacterial motility using optical tweezers

Taejin L Min[1,2], Patrick J Mears[1,2], Lon M Chubiz[3], Christopher V Rao[3], Ido Golding[1,2,4] & Yann R Chemla[1,2,4]

We present a single-cell motility assay, which allows the quantification of bacterial swimming in a well-controlled environment, for durations of up to an hour and with a temporal resolution greater than the flagellar rotation rates of ~100 Hz. The assay is based on an instrument combining optical tweezers, light and fluorescence microscopy, and a microfluidic chamber. Using this device we characterized the long-term statistics of the run-tumble time series in individual *Escherichia coli* cells. We also quantified higher-order features of bacterial swimming, such as changes in velocity and reversals of swimming direction.

Many microorganisms move around by swimming in liquid medium and can modulate their swimming behavior to move up gradients of chemicals, temperature or light. In liquid environments, *Escherichia coli* swims in a random pattern composed of 'runs', in which the cell maintains an approximately constant direction, and 'tumbles', in which the cell stops and randomly changes direction[1]. Runs and tumbles are generated by different states of the motors that rotate the bacterial flagella. Each cell has several flagellar motors that can rotate either clockwise or counterclockwise. When the motors turn counterclockwise, the flagella rotate together in a bundle and push the cell forward. When one or more of the motors turn clockwise, some flagella may break from the bundle and cause the cell to tumble and randomize its orientation. During chemotaxis, *E. coli* biases its 'random walk' based on temporal changes in chemical concentration. When the bacterium moves up a gradient of attractant, it detects an increase in attractant concentration and reduces its probability of tumbling. The result is that the cell tends to continue going up the gradient.

The modulation of bacterial swimming serves as a model system for the way a living cell processes signals from its environment and changes its behavior based on those signals[1,2]. Standard methods for assaying bacterial swimming and chemotaxis typically fall into two categories. The first consists of observing freely swimming cells, typically in a flow-cell setup. Chemoeffector variation is created in space or time[3–5], and the change in swimming behavior is then examined[6,7]. The second type of assay uses cells that are tethered to a surface, usually a microscope slide, so that the rotation of an individual flagellar motor can be followed[8,9].

These approaches have enabled the acquisition of large amounts of data that have yielded important insights into bacterial swimming and its modulation. However, both assays are limited in their ability to quantify whole-cell swimming (**Supplementary Note 1**). Here we describe an optical trap–based assay to investigate cell motility. This assay allowed us to quantify bacterial swimming in a well-controlled environment for durations up to 1 h and at data acquisition rates that are faster than the ~100 Hz flagellar rotation rates. We thus characterized the long-term statistics of the run-tumble time series in individual cells. Moreover, we characterized higher-order features of bacterial swimming, such as changes in velocity and reversals of swimming direction.

RESULTS

Experimental setup

Our single-cell motility assay involves a custom-made instrument combining optical tweezers, light and fluorescence microscopy and a microfluidic chamber (**Fig. 1a**). The optical tweezers consist of two traps generated by two orthogonally polarized beams from a single 1,064-nm diode-pumped solid-state laser[10]. The separation between the two traps is controlled by a piezo-actuated mirror stage. A custom flow-cell (**Supplementary Fig. 1** and Online Methods) serves as the experimental trap chamber and can be displaced relative to the two traps in all directions by a three-axis translational stage. For measurements of bacterial motility, we filled the chambers with a tryptone broth–based 'trapping medium', though other buffers are also appropriate (Online Methods). We injected bacteria into a top 'antechamber' and flowed them through a narrow inlet into the bottom channel, where they were captured by the traps. Trapping a rod-shaped bacterium by each end with two optical traps[11] allowed us to orient the cell at will in the plane of the chamber (**Fig. 1b**). We visualized trapped bacteria either by brightfield or epifluorescence microscopy (**Fig. 1c** and Online Methods).

Despite immobilization by the optical traps, cells displayed motile behavior, evinced by flagellar bundle rotation and counter-rotation ('rolling') of the cell body[12]. This behavior was detected directly and sensitively by the optical traps themselves, by imaging light from both orthogonally polarized trapping beams onto two separate position-sensitive photodetectors. Consistent with

[1]Department of Physics, [2]Center for the Physics of Living Cells, [3]Department of Chemical and Biomolecular Engineering and [4]Center for Biophysics and Computational Biology, University of Illinois at Urbana-Champaign, Urbana, Illinois, USA. Correspondence should be addressed to I.G. (igolding@illinois.edu).

RECEIVED 15 MAY; ACCEPTED 8 SEPTEMBER; PUBLISHED ONLINE 4 OCTOBER 2009; DOI:10.1038/NMETH.1380

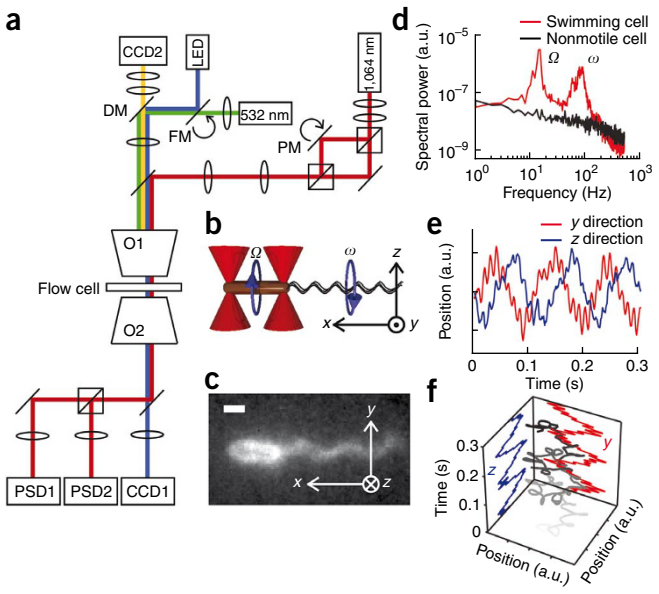

Figure 1 | Combined optical trap and fluorescence microscope setup. (**a**) Instrument layout showing the trapping beam (red), light-emitting diode (LED) illumination path for brightfield imaging (blue), fluorescence excitation beam (green), fluorescence emission (yellow), piezo-actuated mirror (PM), flip-mount mirror (FM), dichroic mirror (DM), microscope objectives (O1 and O2), position-sensitive detectors (PSD1 and PSD2) and charge-coupled device cameras (CCD1 and CCD2). (**b**) Schematic showing optical traps (red cones) and a trapped cell. Circular arrows indicate the rotational direction of the cell body (brown cylinder) and the flagellar bundle (black wavy lines). Also shown is the coordinate axis notation for the optical trap signal. (**c**) Fluorescence image of a Cy3-labeled, optically trapped cell. Scale bar, 1 μm. (**d**) Power spectrum of the optical trap signal from a swimming cell and a nonmotile cell. Swimming cell signal shows oscillatory peaks at 10 Hz and 100 Hz corresponding to body roll (Ω) and flagellar bundle rotation (ω) frequencies, respectively. (**e**) Typical optical trap signal of a swimming cell along *y* and *z* directions. (**f**) A three-dimensional plot (grayscale line) of the swimming cell signal. Color darkens with time. Rotational motion of the cell body (large radius rotations) and the flagellar bundle (small radius rotations) are easily recognizable.

previous reports on optically trapped cells[12,13], power spectra from the position-sensitive photodetector outputs upon trapping of a swimming cell revealed two peaks with frequencies ~100 and ~10 Hz (**Fig. 1d**). These oscillatory signals correspond to flagellar bundle rotation and cell body counterrotation or 'roll'[12,13], respectively (**Fig. 1b**). Our measured flagellar rotation (ω) and body-roll rates (Ω) were consistent with those observed in experiments with freely swimming cells[14], demonstrating that the optical traps did not inhibit motility other than in fixing the cell's position. Although we did not observe cell swimming directly, these oscillation frequencies provide information on the motile behavior of the cell (**Supplementary Note 2**).

In a typical experiment, we trapped an *E. coli* cell (strain RP437, wild-type for chemotaxis[15]) horizontally (defined as *x* in **Fig. 1b**). The motion of each trapped end in the orthogonal plane, along the vertical direction (*y*) and along the optical axis (*z*), was detected by one position-sensitive photodetector and revealed both frequencies of oscillation (**Fig. 1e**). The *y* and *z* components of the low-frequency signal were 90° out of phase, indicating that the cell end moved in a circular trajectory perpendicular to its body axis (**Fig. 1f**). The rotation was clockwise, as measured looking at the tail of the cell in the direction of swimming, consistent with the expected direction of body roll[1]. The higher-frequency oscillatory signal corresponding to flagellar bundle rotation also revealed a circular motion, in the counterclockwise direction, as expected (**Fig. 1f**).

Of primary importance to our work was characterizing the health of the optically trapped cells. The high photon-flux at near-infrared wavelengths generated by the optical traps has been shown to induce photodamage in cells[16,17]. As demonstrated previously[16], this damage can be largely mitigated by trapping cells under reduced oxygen conditions, for instance, by use of an oxygen-scavenging system. We optimized conditions to enhance cell viability in our trap (Online Methods). Under our tryptone broth–based 'trapping medium' (with oxygen scavenger), we found that trapped *E. coli* cells displayed behavior consistent with healthy cells, growing and dividing at a rate comparable to standard values from the literature (~2 h generation time at room temperature[18]) (**Supplementary Fig. 2**). Furthermore, we could follow swimming in individual cells for extended periods of time in the trap (up to ~1 h; data not shown). Our trapping protocol constitutes a substantial improvement over a previously reported trap-based study of bacterial swimming under oxygenated conditions[13], in which cells could be monitored only for very short times (<10 s).

Observation of single-cell run-tumble behavior

Closer examination of swimming traces revealed regions of alternating oscillatory and nonoscillatory ('erratic') signals (**Fig. 2**). By imaging the motion of a Cy3-labeled cell using epifluorescence microscopy and simultaneously monitoring the trap signals generated by this motion, we established that these oscillatory and erratic signals corresponded to runs and tumbles of the cell, respectively. Cell images taken during oscillatory periods (1.2, 2.2, 2.7 and 3.2 s) displayed a well-formed flagellar bundle extending from the tail of the cell as expected for a run, whereas those taken during erratic periods (1.7 s) exhibit a disrupted bundle, indicative of a tumbling conformation[19] (**Fig. 2a**).

To ascertain that the observed run-tumble behavior in trapped cells is physiologically relevant and rule out the possibility of an artifact induced by the optical traps, we performed two control experiments. In the first, we examined the motility of two mutant strains: a *cheY* deletion (strain CR20; see **Supplementary Table 1** for list of strains used in this study), which does not tumble, and a *cheZ* deletion (strain CR33), which mostly tumbles and does not run. Data traces obtained for these mutants displayed the expected phenotypes (**Fig. 3a–c**): 'runners' generated prolonged oscillatory signals, whereas 'tumblers' underwent continuous erratic motion. In the second control experiment, we quantified the run-tumble behavior of strain PS2001-pMS164 (ref. 20), in which a permanently active CheYD13K mutant protein is expressed from an inducible promoter, under the control of isopropyl β-D-1-thiogalactopyranoside (IPTG). This strain allowed us to modulate run-tumble statistics and to compare them to those obtained with our wild-type strain.

To quantify the swimming behavior of optically trapped cells, we developed an automated run-tumble detection routine using the continuous wavelet transform[21] to discriminate regions of oscillatory and nonoscillatory behavior (Online Methods and

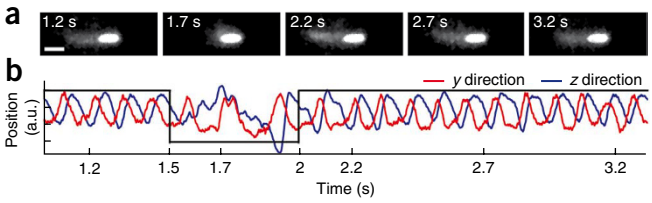

Figure 2 | Direct observation of tumbles in an optically trapped cell. (**a**) Fluorescence images of a trapped cell. Shown in the first frame is the trapped cell body (bright oval shape) and the flagellar bundle (faint cloud) formed to the left of the cell body. The second frame shows the cell tumbling, with the appearance of a disrupted flagellar bundle. Subsequent frames show the reformed flagellar bundle and the running cell. Each frame was obtained by averaging three successive images collected at a rate of 10 Hz, with the marked time point in the middle. Scale bar, 2 μm. (**b**) Optical trap signals in the *y* and *z* directions, recorded simultaneously with the fluorescence images. Black lines delineate the run (high) and tumble (low) periods. Only the low-frequency component corresponding to body roll is shown for clarity.

Supplementary Fig. 3). For a dataset of 43 wild-type cells constituting a total of 5,473 detected run events, our algorithm yielded an average run duration of 3.90 ± 0.30 s (mean ± s.e.m., $n = 43$), within the range of previously reported values (0.8–4 s)[7,20,22]. Analysis of 53 PS2001-pMS164 mutant cells at various induction levels revealed that, as expected, run durations were longer than in wild-type cells at low (1 μM) IPTG concentrations and shorter at high (100 μM) IPTG concentrations. The tumble bias, B—defined as the fraction of time the cell spends tumbling, $B = t_{tum}/(t_{tum} + t_{run})$—exhibited a sigmoidal response to IPTG (**Fig. 3d**). The midpoint of the response was at ~20 μM and the enhancement in bias relative to wild-type cells had a factor of ~4. This behavior is in good agreement with published values[20], confirming our view that tumbles exhibited by trapped *E. coli* represent physiologically relevant events. We note, however, that trapped cells exhibited longer tumble durations than observed in free swimming cells (**Supplementary Note 3**).

Single-cell statistics of motility parameters

The ability to track an individual bacterium for an extended time period (**Fig. 4a**) allowed us to extract single-cell distributions of motility parameters. We determined the cumulative run duration distributions for 43 individual wild-type and 44 individual PS2001-pMS164 cells at a range of induction levels (**Fig. 4b**,**c** and **Supplementary Fig. 4a–d**). Single-cell run-duration distributions were predominantly exponential but also display considerable cell-to-cell variability. To determine more accurately the shape of the distributions, we normalized each curve by the individual-cell mean run duration (as determined by an exponential fit) along the time axis, maximizing the overlap of the individual distributions[7] (**Fig. 4d**,**e**).

By pooling all the normalized data, we characterized the 'average' single-cell run duration distribution (**Fig. 4d**,**e**). Both wild-type and PS2001-pMS164 strain data had exponential distributions at short times, but the former additionally exhibited a pronounced 'heavy tail' corresponding to very long runs, which was much smaller in the mutant strain. The curves for individual wild-type cells also indicate that very long runs are taken by the majority of cells, rather than in a few outliers. Notably, this behavior matched that previously reported in single-motor tethered cell studies[23] and may similarly represent the inherent stochasticity in the chemotactic signaling pathway in wild-type cells. Such a degree of stochasticity was not present in the PS2001-pMS164 strain, in which the concentration of signaling protein CheYD13K is externally controlled. The ability to collect sufficient statistics from individual trapped bacteria provides information not available in population distributions. Note that taking the population averages of the single-cell distributions shown in **Figure 4b** before normalization does not give an accurate representation of the average distribution (**Fig. 4d**), emphasizing the importance of collecting single-cell statistics.

Higher-order features in cell motility

Our preceding analysis of trapped cells characterized their motility in terms of the standard two-state, 'run-tumble' picture. Yet this abstraction of cell swimming is only a first approximation. Researchers in the field have already pointed to aspects of movement beyond this approximation, including changes in cell velocity after a tumble[7], reversal of swimming direction when the flagellar bundle changes its orientation[22,24] and changes in motor and swimming velocity as a function of multiple physiological and mechanical factors[6,13]. Most of these observations, however, were sporadic, limited by the noise or short time duration of available techniques.

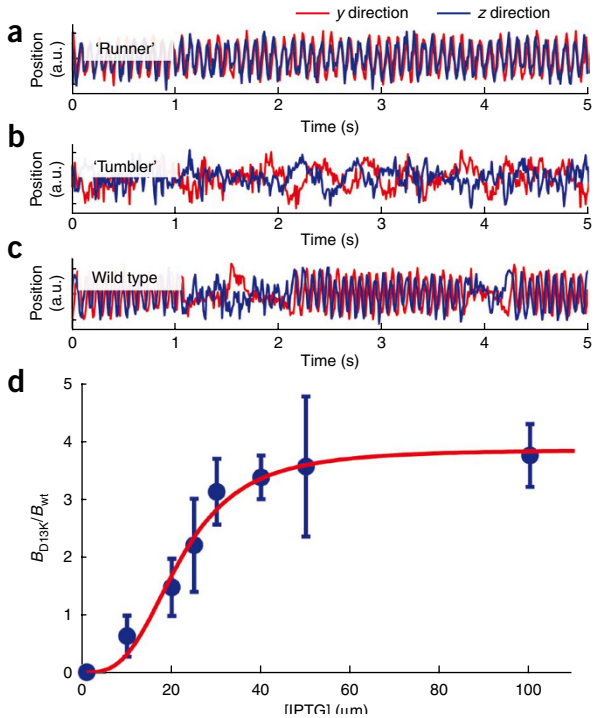

Figure 3 | Run-tumble phenotyping using the optical trapping assay. (**a**) A 'runner' mutant generates predominantly oscillatory signals. (**b**) A 'tumbler' mutant generates predominantly erratic signals. (**c**) A wild-type cell generates oscillatory signals interrupted by intermittent erratic signals. (**d**) Induction response (average tumble bias B_{D13K} of individually trapped cells at various levels of induction, normalized by the average tumble bias of wild-type cells B_{wt}) of the PS2001-pMS164 strain (data points). Higher CheYD13K levels increase the probability of tumbling. Error bars, s.e.m. (n = 6, 8, 8, 5, 13, 4, 3, 6, from lowest to highest IPTG concentration). Fitting to Hill function gives a Hill coefficient of ~3 (red line).

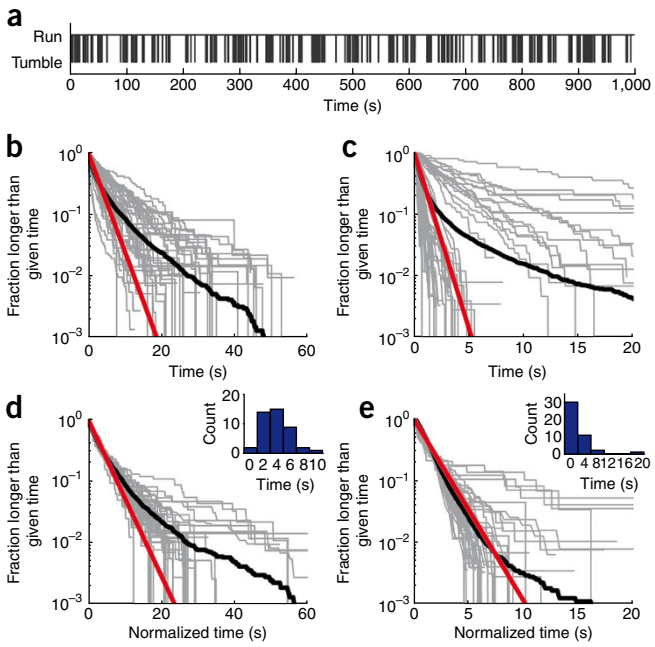

Figure 4 | Run duration statistics in individual bacteria. (**a**) A typical binary time series generated from the swimming signal of a single trapped cell. (**b**,**c**) Cumulative distribution of run durations, comprising 5,473 runs observed in 43 wild-type cells (**b**) and 7,317 runs observed in 44 inducible-bias mutants that showed 20 or more runs (**c**) (black lines). Each gray line shows the run-time statistics from a single cell. The thick black line is the population ensemble. The red line is an exponential fit to 90% of the data, encompassing the shorter events. Each gray line shows the fraction of runs observed from a single cell that were longer than a given time. The red line is an exponential fit to the first decade of the ensemble distribution. (**d**,**e**) Cumulative distribution for wild-type cells (**d**) and inducible bias mutants (**e**) in which individual run duration distributions were scaled so that the mean run duration equals the ensemble mean. This scaling procedure collapses data by effectively removing individual variability, thus revealing the underlying universal behavior in the population ensemble. Inset, histogram of mean tumble durations used in scaling.

Swimming traces collected by our technique also exhibited 'higher-order' swimming dynamics, in particular reversals in phase difference between *y* and *z* signals (**Fig. 5a**), indicating reversals in swimming direction (**Supplementary Fig. 5**) and changes in oscillation frequency (**Fig. 5b**), corresponding to changes in swimming speed[13,14]. To fully analyze such higher-order behavioral patterns, we used the continuous wavelet transform to determine not only the Ω values but also the phase difference, $\Delta\phi$, between *y* and *z* signals at every point in time (**Supplementary Fig. 6**).

We plotted two-dimensional histograms in Ω and $\Delta\phi$ for two representative cells (**Fig. 5c**,**d**). The majority of trapped wild-type cells (42 of 43 cells) exhibited reversals, illustrated by the two peaks along the horizontal $\Delta\phi$ axis in the histograms. Reversals occurred frequently (we detected an average of 21 reversal events per time trace) and exclusively after the cell tumbles, on average one out of every six tumbles, or every 21.2 ± 1.1 s (mean ± s.e.m., $n = 859$) (**Fig. 5e**). In certain cases (29 of 42 reversing cells), reversals were also accompanied by an observable change in Ω (**Fig. 5c**), and thus presumably swimming speed. Notably, a similar analysis of the flagellar bundle rotation signal indicated no corresponding changes in ω in the majority of cells (data not shown). These observations suggest that reversals may be important in the motility of cells (**Supplementary Note 4** and **Supplementary Fig. 7**).

Occasionally (in 6 of 42 cells), cells exhibited noticeable, discrete changes in Ω with no corresponding change in swimming direction (illustrated in the two peaks along the vertical Ω axis; **Fig. 5d**). Changes in speed occurred both spontaneously, without tumbling (69.5%) (**Fig. 5f**) or after a tumble (30.5%). Furthermore, the flagellar bundle exhibited no corresponding changes in ω (data not shown). These observations suggest that speed changes may represent different conformational states of the flagellar bundle (**Supplementary Note 5**).

In addition to these higher-order features, many cells exhibited asymmetric $\Delta\phi$ distributions (**Fig. 5c**,**d**), indicating a bias in swimming direction. Although we found no preferred swimming direction in the cell population, reflecting the fact that our traps do not impose directionality, many individual bacteria did display a distinct bias (**Supplementary Note 6**).

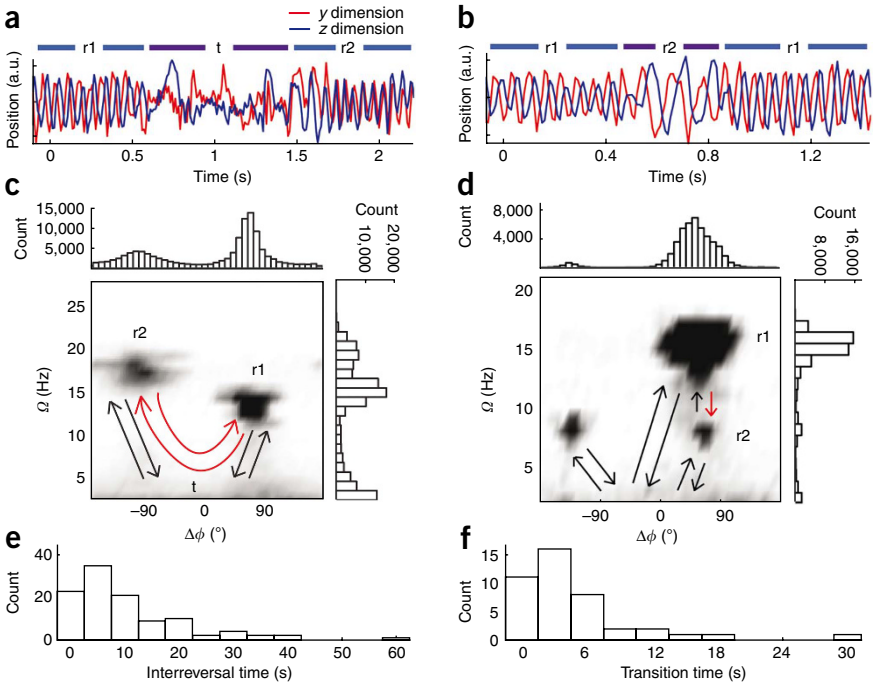

Figure 5 | Higher-order features in cell motility. (**a**) *y*-dimension and *z*-dimension signals showing a reversal in run direction (periods designated r1 and r2) after a tumble (designated t). (**b**) *y*-dimension and *z*-dimension signals showing change in body roll frequency (Ω) (r2) in the middle of a run (r1). (**c**,**d**) Images are two-dimensional histograms of Ω and phase difference between swimming signals in *y* and *z* dimensions ($\Delta\phi$). All possible transitions between different swimming modes are marked by arrows. (**e**,**f**) Waiting time distributions for the transitions highlighted by red arrows in **c** (**e**) and **d** (**f**). Data for **a**, **c** and **e** are from the same cell, and data for **b**, **d** and **f** from another cell.

DISCUSSION

By limiting the physical translocation of the bacterial cell while at the same time allowing high-accuracy measurement of its rotational motion, we followed bacterial swimming for long periods of time with high temporal resolution. The extensive run-tumble statistics thus collected from individual cells expand the range of measured distributions by over an order of magnitude over previous studies[7]. As an example of the consequences of this advance, our wild-type cell run distributions now reveal, to our knowledge for the first time, a pronounced tail similar to that observed in individual flagellar motors[23]. These findings suggest that stochastic variation in the amounts of chemotactic proteins is manifested in the long-term run-tumble behavior of swimming cells.

With our technique we investigated cell swimming beyond the classical, binary run-tumble picture and quantified the statistics of cell reversals, changes in swimming speed and direction bias. Although these features are unique to the swimming behavior of the whole cell (not revealed at the single flagellar motor level), they may also provide insight into the relationship of individual flagella and whole-cell swimming phenotypes. For example, cell reversals may reflect tumbling states in which multiple flagella rotate clockwise and disrupt the flagellar bundle. Tumbles involving a single flagellum are unlikely to induce reversals, as a partial bundle is likely to persist and bias the cell's direction during such tumbles[14]. Changes in swimming speed and bias in swimming direction may similarly reflect different states or spatial arrangements of the flagella.

This technique will be well-suited to investigate chemotaxis in individual cells. A critical requirement for a quantitative characterization of cell chemotactic response is the ability to create an arbitrary stimulus, in the form of spatiotemporally varying chemoeffector concentrations, and to follow the response of the cell in terms of its swimming behavior as well as changes in intracellular parameters such as gene expression. We describe possible approaches to achieving this goal in **Supplementary Note 7**. These advances will enable the development of an integrated device to quantify whole-cell swimming and chemotactic response.

METHODS

Methods and any associated references are available in the online version of the paper at http://www.nature.com/naturemethods/.

Note: Supplementary information is available on the Nature Methods website.

ACKNOWLEDGMENTS

We thank P. Cluzel (Harvard University) for the gift of the PS2001-pMS164 strain and the following people for their generous advice: C. Guet, H. Park, M. McLachlan, K. Neuman, S. Chattopadhyay, W. Ryu, T. Shimizu, R. Segev, G. Ordal, I. Nemenman, T. Emonet and all members of the Golding, Chemla, Rao, Selvin and Ha laboratories. The work was supported by the US National Science Foundation (grant 082265, Center for the Physics of Living Cells). Y.R.C. is supported by Burroughs-Wellcome Fund Career Awards at the Scientific Interface. T.L.M. was supported by National Institutes of Health Institutional National Research Service Award in Molecular Biophysics (PHS 5 T32 GM08276). C.V.R. is supported by National Institutes of Health grant GM054365.

AUTHOR CONTRIBUTIONS

Y.R.C. and I.G. conceived the cell-trapping project. T.L.M. developed the cell-trapping assay. T.L.M. and P.J.M. developed the measurement protocols, performed the experiments and analyzed the data. L.M.C. and C.V.R. constructed and tested bacterial strains used in this study. C.V.R. provided expertise on bacterial physiology and chemotaxis. P.J.M., T.L.M., I.G. and Y.R.C. wrote the paper.

Published online at http://www.nature.com/naturemethods/.
Reprints and permissions information is available online at http://npg.nature.com/reprintsandpermissions/.

1. Berg, H.C. *E. coli in motion*. (Springer, New York, 2004).
2. Alon, U. *An introduction to systems biology: design principles of biological circuits*. (Chapman & Hall/CRC, Boca Raton, Florida, USA, 2007).
3. Brown, D.A. & Berg, H.C. Temporal stimulation of chemotaxis in *Escherichia coli*. *Proc. Natl. Acad. Sci. USA* **71**, 1388–1392 (1974).
4. Khan, S. *et al.* Excitatory signaling in bacteria probed by caged chemoeffectors. *Biophys. J.* **65**, 2368–2382 (1993).
5. Block, S.M., Segall, J.E. & Berg, H.C. Impulse responses in bacterial chemotaxis. *Cell* **31**, 215–226 (1982).
6. Staropoli, J.F. & Alon, U. Computerized analysis of chemotaxis at different stages of bacterial growth. *Biophys. J.* **78**, 513–519 (2000).
7. Berg, H.C. & Brown, D.A. Chemotaxis in *Escherichia coli* analyzed by 3-dimensional tracking. *Nature* **239**, 500–504 (1972).
8. Silverman, M. & Simon, M. Flagellar rotation and the mechanism of bacterial motility. *Nature* **249**, 73–74 (1974).
9. Sowa, Y. *et al.* Direct observation of steps in rotation of the bacterial flagellar motor. *Nature* **437**, 916–919 (2005).
10. Bustamante, C., Chemla, Y.R. & Moffitt, J.R. High resolution dual trap optical tweezers with differential detection. in *Single-Molecule Techniques: A Laboratory Manual* (eds., P. Selvin & T. Ha) 297–324 (Cold Spring Harbor Laboratory Press, Cold Spring Harbor, New York, USA, 2009).
11. Ashkin, A., Dziedzic, J.M. & Yamane, T. Optical trapping and manipulation of single cells using infrared-laser beams. *Nature* **330**, 769–771 (1987).
12. Rowe, A.D., Leake, M.C., Morgan, H. & Berry, R.M. Rapid rotation of micron and submicron dielectric particles measured using optical tweezers. *J. Mod. Opt.* **50**, 1539–1554 (2003).
13. Chattopadhyay, S., Moldovan, R., Yeung, C. & Wu, X.L. Swimming efficiency of bacterium *Escherichia coli*. *Proc. Natl. Acad. Sci. USA* **103**, 13712–13717 (2006).
14. Darnton, N.C., Turner, L., Rojevsky, S. & Berg, H.C. On torque and tumbling in swimming *Escherichia coli*. *J. Bacteriol.* **189**, 1756–1764 (2007).
15. Parkinson, J.S. & Houts, S.E. Isolation and behavior of *Escherichia coli* deletion mutants lacking chemotaxis functions. *J. Bacteriol.* **151**, 106–113 (1982).
16. Neuman, K.C., Chadd, E.H., Liou, G.F., Bergman, K. & Block, S.M. Characterization of photodamage to *Escherichia coli* in optical traps. *Biophys. J.* **77**, 2856–2863 (1999).
17. Rasmussen, M.B., Oddershede, L.B. & Siegumfeldt, H. Optical tweezers cause physiological damage to *Escherichia coli* and *Listeria* bacteria. *Appl. Environ. Microbiol.* **74**, 2441–2446 (2008).
18. Neidhardt, F.C., Ingraham, J.L. & Schaechter, M. *Physiology of the bacterial cell: a molecular approach* (Sinauer Associates, Sunderland, Massachusetts, USA, 1990).
19. Turner, L., Ryu, W.S. & Berg, H.C. Real-time imaging of fluorescent flagellar filaments. *J. Bacteriol.* **182**, 2793–2801 (2000).
20. Alon, U. *et al.* Response regulator output in bacterial chemotaxis. *EMBO J.* **17**, 4238–4248 (1998).
21. Teolis, A. *Computational signal processing with wavelets*. (Birkhäuser, Boston, 1998).
22. Berg, H.C. & Turner, L. Cells of *Escherichia coli* swim either end forward. *Proc. Natl. Acad. Sci. USA* **92**, 477–479 (1995).
23. Korobkova, E., Emonet, T., Vilar, J.M., Shimizu, T.S. & Cluzel, P. From molecular noise to behavioural variability in a single bacterium. *Nature* **428**, 574–578 (2004).
24. Cisneros, L., Dombrowski, C., Goldstein, R.E. & Kessler, J.O. Reversal of bacterial locomotion at an obstacle. *Phys. Rev. E* **73**, 030901 (2006).

ONLINE METHODS

Strains used. The genotypes and sources of all *E. coli* strains used in this study are listed in **Supplementary Table 1**. RP437 is wild type for chemotaxis[15]. CR20 and CR33 are 'runner' (run only) and 'tumbler' (no runs) mutants, owing to *cheY* and *cheZ* deletions, respectively. PS2001 is a strain in which environmental signals are decoupled from the behavior of flagellar motors[20,23]. Tumbling bias in this strain can be adjusted by expressing CheYD13K (ref. 25) from a plasmid (pMS164), under an inducible promoter. As opposed to the wild-type CheY, CheYD13K does not require phosphorylation to be active[23]. Thus, all CheYD13K proteins expressed in the cell can bias flagellar motors for longer clockwise rotation. Clockwise rotation of flagellar motors tends to cause the swimming cell to tumble[1].

Cell growth and media. *E. coli* cells were collected from a single colony on an agar plate and grown overnight in 1 ml tryptone broth (1% (wt/vol) Bacto tryptone and 0.8% (wt/vol) NaCl)[26]. The overnight culture was diluted 100-fold into 1 ml tryptone broth in a 14-ml round bottom Falcon tube and grown for 4.5 h to midlog phase (OD_{600} = ~0.5). The PS2001-pMS164 strain was grown with antibiotics chloramphenicol (34 μg ml^{-1}) and kanamycin (40 μg ml^{-1}), and with 1–100 μM of the inducer isopropyl-β-D-galactopyranoside (IPTG)[20]. All bacteria in this study were grown at 30 °C with 265 rpm rotation[6]. Cells were washed from growth medium by centrifugation (2,000*g*, 10 min) followed by gentle resuspension in trapping medium. Resuspension by pipetting was minimized, as it can cause the flagella to break owing to shear forces.

Trapping medium contained tryptone broth supplemented with 2% (wt/vol) glucose, 100 mM Tris-Cl (pH7.5), and an oxygen scavenging system (100 μg ml^{-1} glucose oxidase and 20 μg ml^{-1} catalase, Sigma; adapted from ref. 27) to reduce trap-mediated oxidative damage to the cells[16]. The oxygen scavenging system was added 2 h before use to reach a steady oxygen level. Resazurin (Sigma) was added (0.0001% (wt/vol)) as an oxygen indicator. Glucose acts as a substrate for the oxygen scavenging system and provides energy for the cells swimming in anaerobic condition[28]. Tryptone broth is an appropriate growth medium for obtaining reproducible cell motility[29]. However, it is not suitable for chemotaxis studies because it contains amino acids that can act as chemoattractants. To demonstrate the future feasibility of chemotaxis measurements using our method, we also examined cell behavior in a 'motility buffer' containing 70 mM NaCl[14], supplemented with 100 mM Tris-Cl, 2% (wt/vol) glucose and the oxygen scavenging system. Trapped cells under these conditions displayed the same behavior as those described in the main text: they remained motile for long durations, exhibited similar flagellar and body rotation rates and tumbled at similar frequencies (**Supplementary Table 2**). A high buffering capacity is necessary to prevent acidification of the medium by gluconic acid, a side product of the oxygen scavenging reactions[30]. Though a 100 mM Tris-Cl buffer is preferable for long-term stability of our trapping medium, a lower molarity is acceptable for shorter time periods (~1 h) if ionic strength is a concern. Cells resuspended in a buffer containing 70 mM NaCl, 10 mM Tris-Cl, 2% (wt/vol) glucose and the oxygen scavenging system were well-behaved in our trap (**Supplementary Table 2**).

Fluorescence labeling of cells. Wild-type cells were labeled with Cy3 monofunctional NHS ester (GE Healthcare) following a previously reported protocol[14]. Cells were grown to midlog phase in tryptone broth and washed twice (1,000*g*, 10 min), with the final resuspension concentrating cells 20-fold in a buffer containing 10 mM KPO_4 (pH 7.0), 70 mM NaCl and 0.1 mM EDTA. Cy3 dye suspended in 25 μl of 1 M $NaHCO_3$ was added to 500 μl of the culture. The labeling reaction was incubated with slow rotation (~10 rpm) at room temperature (~22–27 °C) in the dark for 90 min. The labeled culture was washed once and diluted 100-fold in 1 ml of modified trapping medium. The modified trapping medium contained 50 mM ascorbic acid (Sigma) in place of the oxygen scavenging system. Ascorbic acid is known to quench oxygen radicals and reduce photobleaching[31].

Construction of chemotaxis mutants. The *cheY* and *cheZ* deletion strains were both made using the method presented in ref. 32. In the case of the *cheY* deletion strain, the primers Y_F and Y_R (**Supplementary Table 3**) were used to PCR amplify the chloramphenicol resistance cassette from pKD3 with 40-nt extensions homologous to the flanking regions of the gene to generate an in-frame deletion. Similarly, the primers Z_F and Z_R (**Supplementary Table 3**) were used to generate the *cheZ* deletion strain. In the case of the *cheY* deletion, the antibiotic resistance cassette was removed by passing pCP20 through the strain.

Combined optical tweezers and fluorescence microscope. A detailed description of the optical tweezers design can be found elsewhere[10]. Briefly, the optical tweezers component consisted of two orthogonally polarized beams from a single 5-W, 1,064-nm diode-pumped solid-state laser (BL-106C; Spectra-Physics). Both beams were tightly focused to generate optical traps by a ×60, water-immersion (1.2 numerical aperture (NA)) microscope objective (Nikon). The separation between the two traps was controlled by a piezo-actuated mirror stage (Nano-MTA; Mad City Labs). An identical objective lens collected transmitted light for position detection and bright-field imaging. A custom flow cell (see below) positioned between the two objective lenses served as the experimental chamber and could be displaced relative to the two traps in all directions by a motorized three-axis translational stage (ESP300; Newport). Cell motion was detected directly by the optical traps themselves, using the standard optical techniques known as back-focal plane interferometry, in which trap light scattered by an object relays the object's position relative to the trap in all three directions. Epifluorescence excitation in widefield configuration was provided by a 30-mW, 532-nm diode laser (TECGL-30; World Star Tech). Emitted fluorescence light passed through a dichroic mirror (Di01-R532-25×36, single-edge 532-nm laser dichroic; Semrock), a ×5 beam expander (for additional image magnification) and an emission filter (FES0900, band-pass 540–870 nm; Thorlabs) before being imaged onto an intensified charge-coupled device (I-PENTAMAX; Princeton Instruments). When displaying the fluorescence images, which were taken at 10 frames per second, the contrast was adjusted to maximize the contrast between the flagella and the background, and opening/closing morphological operations were applied to smooth out the noise. Opening first erodes and then dilates the image using a structure element, which in our case was a disk with a 3-pixel radius. Erosion takes darker pixels and expands them

doi:10.1038/nmeth.1380

to the neighboring pixels using the structure element. Dilation does the same with lighter pixels. Closing performs a dilation followed by an erosion. For more information on these morphological operations, see ref. 33. Each frame shown in **Figure 2a** and **Supplementary Fig. 5** is an average of three such images.

Construction of the flow cell. Glass coverslips (Fisher, number 1) were sonicated in dry acetone for 5 min and rinsed with deionized water. Flow channel patterns were cut out from Nescofilm (Karlan) and placed in between two coverslips, one of which had custom-drilled holes (0.05-inch diameter) for inlets and outlets. A short piece of glass capillary (100 μm outer diameter) was positioned near the experimental region as a spacer and a point of reference. The Nescofilm flow channel pattern was bonded to coverslips by melting on a hot plate for 4 min. The completed flow cell was inserted into a custom metal frame where inlet and outlet tubing were screwed on for a tight seal (**Supplementary Fig. 1**).

Optical trapping assay. *E. coli* cells suspended in trapping medium at a low density (OD_{600} = ~0.01) were injected into the top 'antechamber', and flowed through an inlet into the bottom channel containing blank trapping medium. Cells were initially trapped by a single beam along the beam axis, and the second beam was repeatedly brought near the first and pulled away until the two ends of the rod-shaped cell were held by each trap. The separation between the two traps was adjusted until it appeared roughly equal to the cell length. We used 50 mW of trapping power at the sample plane in each trap, sufficient to stably trap and manipulate the cells yet low enough to minimize photodamage. Before data acquisition, the trapped cell was moved sufficiently far away from the connecting region between the top and the bottom channels to prevent possible interruptions by other cells in the flow cell. In addition, the use of water-immersion objectives to form our traps allowed us to position cells far from the sample chamber surfaces (50 μm), minimizing potential cell-surface interactions.

Two-dimensional swimming assay. A small drop (~5 μl) of trapping medium containing *E. coli* cells at OD_{600} of ~0.1 was placed on a coverslip (Fisher; number 1.5) and spread evenly by gently covering with a 22 mm × 22 mm coverslip (Fisher; number 1) from the top[20]. Care was taken to prevent formation of air bubbles. Coverslips were used directly out of the box[19]. To prevent drift owing to evaporation, open sides were sealed with molten wax. Two-dimensional (2D) swimming of *E. coli* cells confined in the resulting ~10-μm-thick fluid chamber was observed in phase contrast with a ×10 objective (Nikon Eclipse TE2000-E). Thirty-second video images were taken at 30 frames per second at various locations on each slide[20].

Run-tumble analysis of optical trap data. All routines for analyzing optical trap data were written in Matlab (Mathworks). Raw data obtained at 1,000 Hz sampling frequency were low-pass–filtered to 100 Hz, and the amplitude was normalized in nonoverlapping 1-s windows. Two separate sets of *y* and *z* signals obtained from the two ends of the cell body were combined by taking the difference for enhancement in signal-to-noise ratio[34]. Motion of the cell in the *x* direction was also detected by the position-sensitive photodetector but was more inconsistent. We believe this is because the cell trajectory was predominantly in the orthogonal *y*–*z* plane. Thus, signals along the *x* direction were not used in our analysis. Using the *y* and *z* signals, the peak frequency component (Ω) at each time point was obtained from a continuous wavelet transform. This method is preferable to a Fourier transform over a running time window. Whereas the Fourier transform is limited by the tradeoff between temporal and spectral resolution for a given window size (a larger time window results in high frequency resolution but low time resolution and vice versa), the continuous wavelet transform does not require a characteristic window size. Instead, this transform makes use of a 'mother wavelet' that can be scaled and shifted to find the best match for the data trace at each time point. The scale can then be converted to a corresponding frequency. Our wavelet analysis was performed using the complex Morlet mother wavelet in a linearly scaled frequency range of 2–40 Hz[21]. A typical result is shown in **Supplementary Figure 3**. Runs and tumbles were distinguished by applying a single threshold value to the Ω time trace. The threshold was determined by examining the distribution of Ω and finding the local minimum between peaks corresponding to run and tumble (**Supplementary Fig. 3b**). For cases in which a clear local minimum could not be found, an arbitrary threshold of 4 Hz was applied. Detected runs and tumbles that were shorter than 100 ms were removed, as our detection limit was expected to be one cycle in the sinusoidal pattern of the running cell (10 Hz body-roll frequency is taken as an arbitrary standard). We obtained two separate binary traces from the signals in *y* and *z* directions from each cell. The same threshold value was used for both *y* and *z* directions, and the two resulting binary traces were combined using an 'and' gate to produce a single binary trace for the cell. Various swimming parameters of individual cells were estimated from the resulting binary trace. For instance, the mean run and tumble durations were determined by fitting the run and tumble duration distributions with exponential distribution functions.

Analysis of higher-order features in trap data. In addition to the peak frequency component (Ω), the corresponding phase (ϕ) at each time point was obtained from the continuous wavelet transform of the swimming signals in *y* and *z* directions (**Supplementary Fig. 6b–d**). We manually examined 2D histograms of Ω and $\Delta\phi$ (phase difference between the *y* and *z* directions) to define different swimming states as follows (i) A threshold in Ω that divides the tumble state from the run states was determined from the local minimum in the Ω histogram. (ii) A threshold in $\Delta\phi$ that divides the run states into runs in two opposite directions was determined as the mid-point between the two peaks in the $\Delta\phi$ histogram. (iii) If multiple run states were clearly visible from the 2D histogram in either of the run directions, a threshold dividing those states was determined as the midpoint between the center points in the 2D histogram. A typical result of these procedures is shown in **Supplementary Figure 6a**. Each time point in the data trace was then assigned to a particular state according to Ω and $\Delta\phi$ values (**Supplementary Fig. 6e**). Detected events shorter than 100 ms were removed for the same reason as discussed above. Unlike the case of two-state analysis, we did not obtain two separate multistate traces from the *y* and *z* directions. Instead, the average Ω of the *y* and *z* directions was used.

Analysis of two-dimensional swimming videos. The field of view of video images was 512 × 512 pixels, covering

approximately 320 μm × 320 μm. Images were analyzed using a custom routine written in Matlab, loosely based on previously reported algorithms[20,35]. Images were adjusted for contrast and a threshold was applied to discriminate cells as black objects against a white background. Contiguous black objects between 3–30 pixels in size were identified as cells, and their centroid and long-axis orientation were determined. Trajectories connecting the cell positions in successive image frames were tracked by matching each cell with one cell in the next frame that was within 5 pixels. A trajectory was terminated if there were no cells or multiple cells connected in the next frame. Trajectories shorter than 3 μm in contour length or 1.33 s in duration were discarded. The remaining trajectories were filtered using a modified median filter following the description in ref. 20. The filtered trajectories were then analyzed to determine run-tumble statistics, distributions of angle changes, run speed and other parameters of potential interest. Of particular interest were run and tumble durations. Tumbles were identified by setting thresholds in both linear velocity and angular velocities. First, the 'average speed' of a cell was defined by sorting the linear velocity values for each cell, excluding the top and bottom 10%, and taking the mean of the remaining velocities. The tumble threshold was then defined as any drop in linear velocity below half the 'average speed' of the cell, and an increase in angular velocity to three times the average angular velocity (similar to the algorithm used in ref. 35). The end of each tumble was determined by comparing the speed after a tumble to the 'running speed', which was defined as the mean of the fastest 10% of speeds in a trajectory[20]. After initiation of a tumble, a standard student's *t*-test was applied to compare a moving 3-point window of speeds to the running speed. When the *t*-test had a *P* value higher than 0.05, the ends of tumbles were scored.

25. Korobkova, E.A., Emonet, T., Park, H. & Cluzel, P. Hidden stochastic nature of a single bacterial motor. *Phys. Rev. Lett.* **96**, 058105 (2006).
26. Saini, S., Brown, J.D., Aldridge, P.D. & Rao, C.V. FliZ. is a posttranslational activator of FlhD4C2-dependent flagellar gene expression. *J. Bacteriol.* **190**, 4979–4988 (2008).
27. Selvin, P.R. *et al. In vitro* and *in vivo* FIONA and other acronyms for watching molecular motors walk. in *Single-Molecule Techniques: A Laboratory Manual* (eds., Selvin P. and Ha T.) 37–71 (Cold Spring Harbor Laboratory Press, Cold Spring Harbor, New York, USA, 2008).
28. Adler, J. & Templeton, B. The effect of environmental conditions on the motility of Escherichia coli. *J. Gen. Microbiol.* **46**, 175–184 (1967).
29. Berg, H.C. & Turner, L. Chemotaxis of bacteria in glass capillary arrays. Escherichia coli, motility, microchannel plate, and light scattering. *Biophys. J.* **58**, 919–930 (1990).
30. Joo, C. & Ha, T. Single-molecule FRET with total internal reflection microscopy. in *Single-Molecule Techniques: A Laboratory Manual* (eds., Selvin P. and Ha T.) 3–36 (Cold Spring Harbor Laboratory Press, Cold Spring Harbor, New York, USA, 2008).
31. Dijk, M.A., Kapitein, L.C., Mameren, J., Schmidt, C.F. & Peterman, E.J. Combining optical trapping and single-molecule fluorescence spectroscopy: enhanced photobleaching of fluorophores. *J. Phys. Chem. B* **108**, 6479–6484 (2004).
32. Datsenko, K.A. & Wanner, B.L. One-step inactivation of chromosomal genes in *Escherichia coli* K-12 using PCR products. *Proc. Natl. Acad. Sci. USA* **97**, 6640–6645 (2000).
33. Gonzalez, R.C., Woods, R.E. & Eddins, S.L. *Digital Image Processing Using MATLAB* (Pearson/Prentice Hall, Upper Saddle River, New Jersey, USA, 2004).
34. Moffitt, J.R., Chemla, Y.R., Izhaky, D. & Bustamante, C. Differential detection of dual traps improves the spatial resolution of optical tweezers. *Proc. Natl. Acad. Sci. USA* **103**, 9006–9011 (2006).
35. Amsler, C.D. Use of computer-assisted motion analysis for quantitative measurements of swimming behavior in peritrichously flagellated bacteria. *Anal. Biochem.* **235**, 20–25 (1996).

doi:10.1038/nmeth.1380